Exploring pathways to reactor-relevant integrated scenarios in MAST-U through targeted trade-offs in plasma shape, stability, and density control

S. Henderson[1], O. Bardsley[1], C. Beckley[1], S. Blackmore[1], J. Harrison[1], H-T. Kim[1], K. Kirov[1], B. Patel[1], D. Morbey[1], S. Saarelma[1], Z. Stancar[1], A. Thornton[1], C. Vincent[1], H. Anand[2], K. Imada[3], D. Frattolillo[4], and the MAST Upgrade team[5]

[1] UKAEA, Culham Campus, Abingdon, Oxfordshire OX14 3DB, UK
[2] General Atomics, PO Box 85608, San Diego, CA 92186-5608, USA
[3] York Plasma Institute, Department of Physics, University of York, Heslington, York YO10 5DD, UK
[4] CREATE Consortium, Via Claudio 21, 80125 Napoli, Italy
[5] See author list of J.R. Harrison et al 2026 Nucl. Fusion 66 116005

Introduction

Previous high-performance MAST-U scenarios [1] have typically used early off-axis (SW) and delayed on-axis (SS) neutral-beam injection (NBI), producing a relatively quiescent early phase before a performance-limiting 2/1 mode develops shortly after the L-H transition, degrading confinement, reducing core rotation, and capping stored energy and β_N. Optimisation is further complicated by internal reconnection events (IREs) shortly after flat-top and before the L-H transition, whose variable timing affects beam coupling and repeatability. This work extends previous scenario development by testing whether more robust high-performance plasmas can be obtained by optimising multiple actuators, including NBI timing, fuelling, divertor closure, and plasma shaping. Here, reactor-relevant high performance means $\beta_N>3$, $\beta_{e,core}>5\%$, confinement approaching $H_{98(y,2)}\sim1$, and strong shaping with $\kappa>2$. With the heating power currently available in MAST-U, detached SXD operation is routinely achieved. The focus here is on how divertor closure and fuelling influence pedestal impurity accumulation, ELM stability, and core MHD.

Neutral Beam Timing

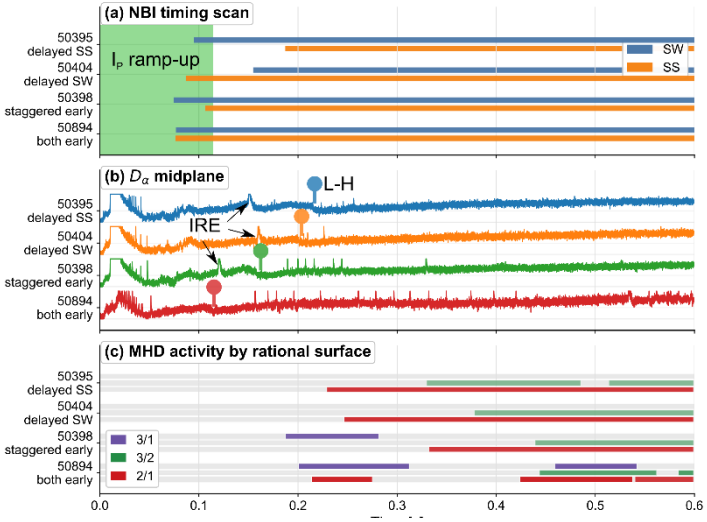

Figure 1: Neutral beam timing scan.

The beam-timing scan tested whether earlier NBI could improve the early scenario trajectory by advancing the L-H transition, building pedestal pressure and bootstrap current earlier, and supporting lower l_i for improved access to high-κ operation. It also assessed whether NBI timing could suppress the IRE and produce a higher q-profile to delay or mitigate the 2/1 mode. The I_P flat-top time started at ~120 ms in all cases shown.

The results are shown in Figure 1. The delayed SS case produced the least favourable trajectory, with the latest L-H transition and earliest 2/1 onset, while delaying the less core-heating off-axis SW beam gave a modest improvement. Earlier staggered beam timing further advanced H-mode access and extended the high-performance phase, but the strongest improvement was obtained when both beams

were injected early. This mitigated the IRE after flat-top and gave the latest 2/1 onset, producing the longest high-performance phase. However, although the both-early case was concluded to be the most favourable access trajectory, it also exposed a new limitation: an early 3/1 mode associated with impurity accumulation near the pedestal.

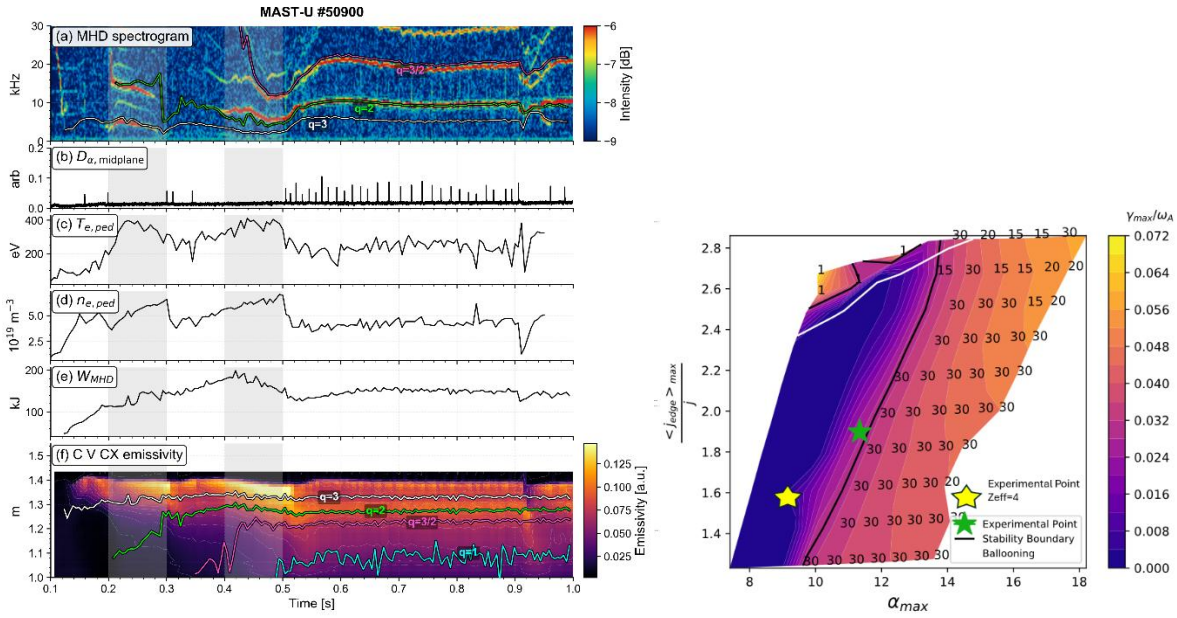

Figure 2: Time evolution of magnetic activity, Dα, pedestal temperature and density, stored energy, CXRS C V emission, and peeling-ballooning stability, showing the pedestal response during the 3/1 and 2/1 island phases.

Density and Impurity Control

Figure 2 highlights the next problem associated with early NBIs: once high-performance H-mode is reached, coherent MHD appears close to the pedestal and fundamentally changes the pedestal evolution. The spectrogram shows two distinct island phases, an early phase associated with the 3/1 mode and a later phase associated with the 2/1 mode, both located close to the pedestal region of φ_N~0.95 (R~1.37 m). The midplane D_α trace shows that each phase coincides with an ELM-free period. During both island phases, the pedestal electron temperature and density increase, which would normally suggest an improving pedestal, but the stored energy either flattens or decreases. This indicates that the response is not simply stiff transport, where higher pedestal temperatures translate into higher global confinement, but is instead coupled to the MHD state, with islands likely cooling the core while heating and fuelling the pedestal. The CXRS C V emission shows impurity accumulation near the pedestal.

The stability analysis shown in Figure 2 provides a possible explanation for the ELM-free phase. If island-driven impurity redistribution increases pedestal Z_{eff}, this may contribute to ELM stabilisation: at Z_{eff}=2, the pedestal is close to the peeling-ballooning boundary, consistent with ELMy behaviour, while Z_{eff}=4 moves it into an ELM-stable region. The impurity accumulation associated with the pedestal islands could therefore explain why these phases become ELM-free. However, further analysis is required to confirm this hypothesis.

Fuelling and divertor closure

Large transients (for example, IREs or large ELMs) expel pedestal density and impurities, sometimes transiently improving beam coupling and rotation, but they are not reliable

operating paths because they depend on uncontrolled events and reduce reproducibility. Additional D_2 puffing provides a more controlled route to mitigating IREs but cools the pedestal and lowers confinement. Changing the closure of recycled-neutral pathways from the divertor to the upstream plasma provides a similar, but more subtle, actuator for modifying the upstream plasma.

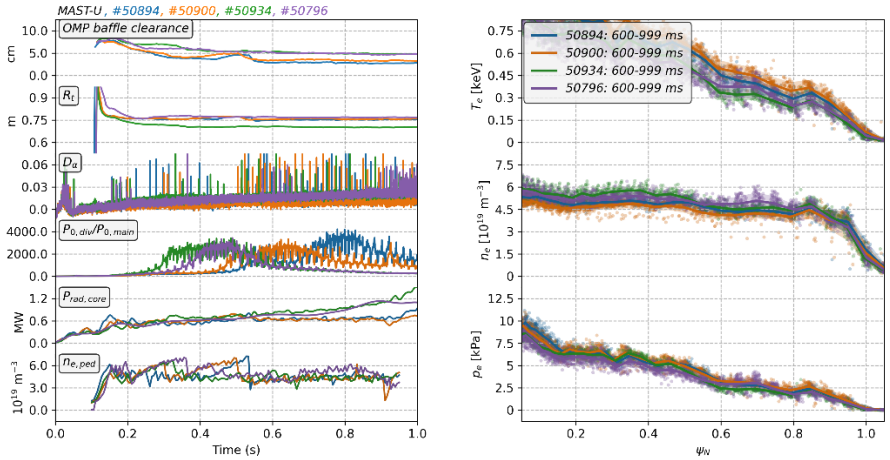

Figure 3: Comparison of midplane-mapped baffle clearance, strike-point position, Dα, pressure-gauge response, core radiation, pedestal density, and TS profiles for different divertor closure conditions.

The divertor closure scan is shown in Figure 3. The top panels show the baffle clearance, defined as the separation between the separatrix and the baffle nose mapped back to the outer midplane, and the target strike-point position. The blue and orange cases maintain a baffle clearance of ~3–4 cm, while the green and purple cases operate with a larger clearance of ~5 cm. In the green case, the strike point is also moved further inward into a more open, less baffled geometry. The higher background midplane D_α signal in the green and purple cases indicates increased neutral levels in the main chamber, consistent with FIG pressure measurements showing stronger divertor-to-midplane compression in the more closed blue and orange cases later in the discharge. Core radiation rises significantly in the more open green and purple cases, while the Thomson scattering data shows consistently higher pedestal electron temperature in the more closed blue and orange cases after the 2/1 mode. The pedestal density evolution shows that the early accumulation phase associated with the 3/1 mode is only weakly affected by divertor closure, suggesting that this phase is primarily set by other actuators. In contrast, the later density and impurity accumulation associated with the 2/1 mode onset is reduced in the more open green and purple cases. The resulting picture is therefore a trade-off: stronger closure improves neutral compression and later pedestal temperature but can also increase sensitivity to MHD, similar to the effect observed when fuelling is reduced.

The optimum clearance does however pose a risk for enhanced ELM sputtering, particularly in high-frequency Type III regimes. The Super-X divertor (SXD) reduces upstream sensitivity to baffle clearance, thus allowing the SOL to be moved further from the baffle while maintaining favourable divertor conditions. The SXD is therefore concluded to be the most robust option.

Plasma shaping

The final optimisation step was to assess whether stronger plasma shaping could improve robustness to the MHD-linked impurity accumulation identified above. Figure 4 compares κ~2.1 and κ~2.5 scenarios with different current ramp rates. The blue and orange cases use fast

current ramp-up at medium and high κ, respectively. However, stronger fuelling was required to suppress IREs that were prevalent throughout the flat-top at κ~2.5. A slower ramp-up scenario shown in green enabled IRE suppression with lower fuelling rates similar to the κ~2.1 scenario. The κ~2.1 scenario is an SXD, whereas κ~2.5 scenarios use a conventional divertor, due to difficulties maintaining the SXD configuration at the l_i values typical of these scenarios.

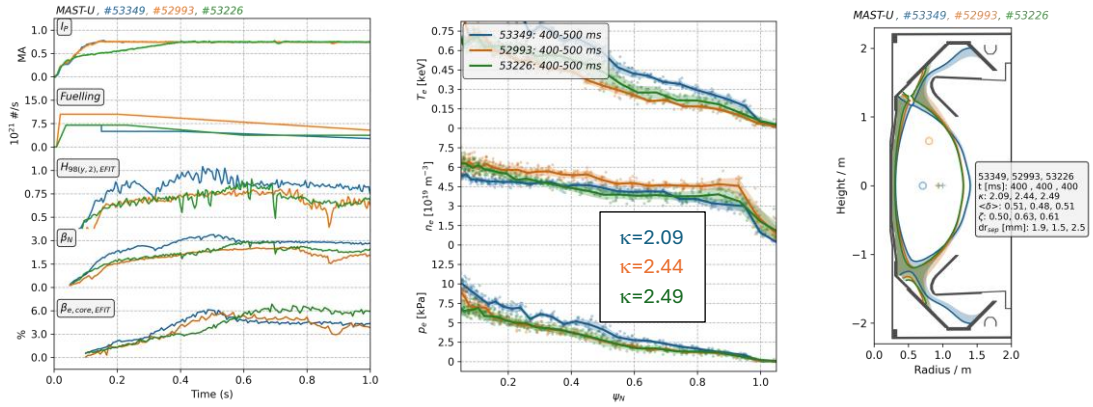

Figure 4: Comparison of current ramp-up, shaping, fuelling, confinement, β_N, and core $\beta_{e,core}$, Thomson scattering profiles, and equilibrium for medium- and high elongation scenarios.

The κ~2.5 scenario avoids the strong pedestal density and impurity accumulation events observed in the κ~2.1 scenario and does not show a core MHD event that significantly degrades the performance. However, this improved robustness comes from a lower performance starting point. The κ~2.5 scenarios reach only $H_{98(y,2)}$~0.75 and β_N~2.5, compared with $H_{98(y,2)}$ peaking near 1 and remaining at ~0.8 after the 2/1 mode in the κ~2.1 scenario, with β_N~2.5. Although $\beta_{e,core}$ reaches a higher steady value of ~6% at κ~2.5, Thomson scattering shows a substantially cooler pedestal temperature and lower pedestal pressure profile than κ~2.1. Therefore, high κ improves MHD robustness but does not yet improve integrated performance; understanding the reasons for the lower pedestal temperature and worse confinement is a key future objective.

Summary

No single scenario was able to simultaneously optimise confinement, β_N, MHD resilience, and core $\beta_{e,core}$. The best confinement was obtained at more moderate shaping, where the most effective strategy was to optimise performance during, rather than fully avoid, the 2/1 phase. Stronger shaping reduced the severity of core MHD and produced a higher $\beta_{e,core}$, but with lower overall confinement and β_N. Future MAST-U experiments with higher auxiliary heating and plasma current will test whether these can be integrated into a single scenario.

References

[1] A. Thornton et al. 29th IAEA Fusion Energy Conference (FEC 2023) Development of integrated plasma scenarios in MAST-U, EX/P4-2, London, UK

Acknowledgements

This work has been (part-) funded by the EPSRC Fusion Grant 2022/27 [grant number EP/W006839/1]. To obtain further information on the data and models underlying this paper please contact PublicationsManager@ukaea.uk